JOURNAL OF Materials CHEMISTRY

Chemical interactions between strontium-doped praseodymium manganite and 3 mol% yttria-zirconia

Jin-Ping Zhang,*[a] San-Ping Jiang,[b] Jonathan G. Love,[a] Karl Foger[a] and Sukhvinder P. S. Badwal[b]

[a] *Ceramic Fuel Cells Limited, 170 Browns Road, Noble Park, Vic. 3174, Australia*
[b] *CSIRO, Manufacturing Science & Technology, Private Bag 33, Clayton South MDC, Clayton, Vic. 3169, Australia*

Received 27th July 1998, Accepted 14th September 1998

The interfacial reaction between $(Pr_{0.8}Sr_{0.2})_yMnO_3$ (PSM, $y=0.9$, 1.0, 1.05) film and 3 mol% yttria tetragonal zirconia (TZ3Y) substrate has been studied at 1200 and 1400 °C in air. A diffusion layer of Pr and Mn in zirconia, which was identified to be a cubic phase of zirconia, was detected in all specimens. When the solubility limit of Pr ions in the cubic zirconia was reached, a pyrochlore phase, $Pr_2Zr_2O_7$, was formed. A delay for the formation of pyrochlore phase was observed for the A-site sub-stoichiometric and stoichiometric PSM at 1200 °C. For the A-site over-stoichiometric PSM, a Pr-rich $(Pr,Zr)O_x$ phase was detected at the interface besides the pyrochlore phase. At 1400 °C, a relatively thick layer of pyrochlore phase was formed after 24 hour heat treatment in all specimens. The amount of the pyrochlore phase formed at the interface depends on the A-site stoichiometry of perovskite in the initial stage. The growth of the pyrochlore layer after the initial stage, however, appears to be determined by contact area between PSM and the substrate.

1 Introduction

Doped perovskite oxides and yttria-zirconia (YSZ) are commonly used as cathode and electrolyte materials respectively in solid oxide fuel cells (SOFCs) operating at temperatures of around 900–1000 °C.[1,2] Interfacial reactions between the cathode [especially in Sr-doped lanthanum manganite (LSM)] and YSZ, have been studied extensively at high temperatures, and the reaction products have been well characterised and documented.[3–7] The stoichiometric LSM reacts with YSZ extensively at temperatures above 1200 °C,[6–10] forming lanthanum zirconate $La_2Zr_2O_7$ and/or strontium zirconate $SrZrO_3$ phases at the interface depending on the La/Sr ratio at the A-site. The interfacial reactions have also been reported at lower temperatures by some authors (1150, 1100[4,11] and 1000 °C[12]). It is generally known that an A-site deficient LSM suppresses the formation of $La_2Zr_2O_7$.[4,6,11,13] The formation of zirconates at the interface is detrimental to the performance of a solid oxide fuel cell system, causing substantial increase in the overpotential and resistivity at the cathode/electrolyte interface.[14]

Owing to severe corrosion of stack components, high cost and degradation of stack performance, it is necessary to lower the operating temperature of SOFCs from 900–1000 °C to the intermediate range 700–800 °C.[2] One of the requirements for lowering the operating temperature is to develop a new cathode material which has reasonably low overpotential losses in the 700–800 °C temperature range. Ishihara *et al.*[15] studied the electrochemical behaviour of the Sr-doped praseodymium manganite (PSM) and found that the overpotential losses for PSM were significantly lower than those of other Sr-doped lanthanide manganites at intermediate operating temperatures. Therefore the material is a potential cathode for intermediate temperature SOFC operation. However, information on interactions between PSM and YSZ is scarce. Wen *et al.*[16] sintered a PSM and YSZ powder mixture at 1000 °C for 100 h and did not detect any interfacial reactions. In order to examine interfacial reactions between PSM and YSZ, a higher heat treatment temperature (≥1200 °C), similar to those used for the LSM/YSZ system in most investigations, may be required. In the present study, the microchemical and microstructural changes between porous $(Pr_{0.8}Sr_{0.2})_yMnO_3$ ($y=0.9$, 1.0, 1.05) film and 3 mol% Y_2O_3-ZrO_2 (TZ3Y) electrolyte have been investigated in air at 1200 and 1400 °C. Although not much information is reported on interactions between TZ3Y and LSM, this electrolyte composition, despite its low conductivity, is of considerable interest to many SOFC technology developers, because its mechanical strength is high and it is easy to fabricate very thin (60–70 μm) sheets of this material (as opposed to 150 μm for the 8 mol% Y_2O_3-ZrO_2).

2 Experimental

The PSM powders with composition $(Pr_{0.8}Sr_{0.2})_yMnO_3$ ($y=$ 0.9, 1.0 and 1.05, coded hereafter PSM-A, PSM-B and PSM-C respectively) were prepared by co-precipitation followed by calcination at 1000 °C for 4 h in air. The value of y is used to indicate the stoichiometry of the perovskite phase for convenience only and no assumption has been made that it is a single phase material. The electrolyte substrate TZ3Y, 20 mm in diameter and 150 μm in thickness, was prepared from 3 mol% Y_2O_3-ZrO_2 (Tosoh Corporation, Japan) by tape casting and sintering at 1500 °C. The PSM was screen-printed (*ca.* 40 μm thick) on the TZ3Y substrate and sintered at 1200 °C for 4, 24 or 168 h. Another batch was sintered at 1400 °C for 24 h. The heat treatment temperature of 1200 °C has been commonly used in the LSM/YSZ system for the investigation of the interfacial reaction. The 1400 °C temperature was used to accelerate the solid state reaction for a more conspicuous observation of the interactions between PSM and TZ3Y.

PSM powders after calcination were characterised by X-ray diffraction (XRD) for phase analysis and by scanning electron microscopy (SEM) for powder morphology. After heat treatments, the reaction couples were carefully fractured and in some cases polished cross-sections were prepared. Both fractured face and polished cross-sections were examined with SEM. X-Ray energy dispersive spectroscopy (EDS) was used to study the elemental distribution in the PSM/TZ3Y interface region. In some samples, PSM was carefully removed from the TZ3Y substrate and the exposed TZ3Y surface was examined with XRD and SEM/EDS. A Siemens D500 X-ray diffractometer (Siemens, Germany) with Cu-Kα radiation and

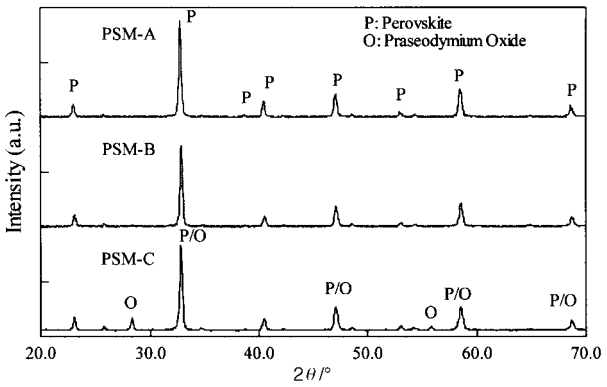

Fig. 1 XRD patterns of the powders calcined at 1000 °C showing that PSM-A and PSM-B are relatively pure perovskite, while PSM-C contains the major phase perovskite and a small amount of praseodymium oxide.

a Leica 360 field emission SEM (Cambridge, UK) equipped with an Oxford Link EDS system were used for specimen characterisation.

Identification of phases from XRD patterns was based on the JCPDS-ICDD database. The Rietveld method,[17] a technique for crystal structure refinement from powder diffraction data, was used in the current study to analyse zirconia phases at the PSM/TZ3Y interface. The Rietveld refinement was performed using the program LHPM1.[18]

3 Results

XRD traces of powders calcined at 1000 °C are displayed in Fig. 1. The diffraction peaks marked 'P' in Fig. 1 are of perovskite, and those marked 'O' belong to praseodymium oxide Pr_6O_{11}. The stoichiometric PSM-B and the A-site substoichiometric PSM-A powders are relatively pure perovskite while A-site over-stoichiometric PSM-C powder contains a small amount of praseodymium oxide besides the major perovskite phase. A few minor unidentified reflections are also noticed in all the traces.

The powder morphology of PSM-A, PSM-B and PSM-C is about the same after calcination at 1000 °C for 4 h. The PSM particle size was in the range 0.1–0.2 μm.

(1) Reaction products after heat treatment at 1400 °C

Two reaction layers were identified between TZ3Y and PSM. Fig. 2 displays the backscattered electron micrographs taken from a polished cross section of the PSM/TZ3Y interface after heat treatment at 1400 °C for 24 h. The first reaction layer (marked L1 in Fig. 2) can be clearly observed in these micrographs. Pr and Zr were identified by EDS analysis as the major elements in the reaction layer. To identify the phase of the reaction layer, PSM was removed carefully by scraping and the exposed surface of the reaction layer was examined by XRD. A representative XRD trace from the reaction layer on TZ3Y substrate which was in contact with PSM-C is presented in Fig. 3 with the identification of each reflection. The major reflections (marked 'X' in Fig. 3) match with those of the pyrochlore phase, $Pr_2Zr_2O_7$ (ICDD file No.: 19-1021), except that the intensity of the reflection (400) ($2\theta = 33.45°$) is about twice that reported in 19-1021. This probably is due to the preferred orientation. Thus both XRD and EDS analysis results confirm that the major phase in the reaction layer 'L1' is $Pr_2Zr_2O_7$, the pyrochlore phase. Some minor reflections in Fig. 3 arise from the substrate TZ3Y, and the perovskite powder left-over after scraping.

The average thickness of the praseodymium zirconate layer determined from backscattered electron micrographs varied with the compositions of PSM. It was about 9.5 μm thick

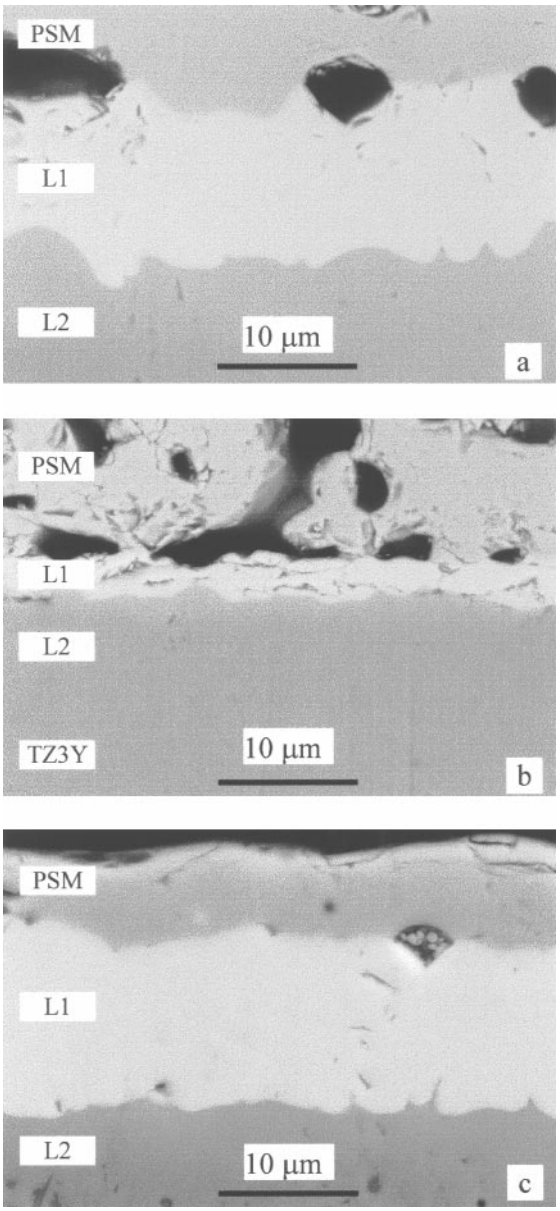

Fig. 2 The backscattered electron micrographs of the polished cross section of the interfaces after 24 h at 1400 °C: (a) PSM-A/TZ3Y; (b) PSM-B/TZ3Y; (c) PSM-C/TZ3Y. 'L1' and 'L2' refer to the pyrochlore layer and the Pr- and Mn-diffused zirconia layer respectively.

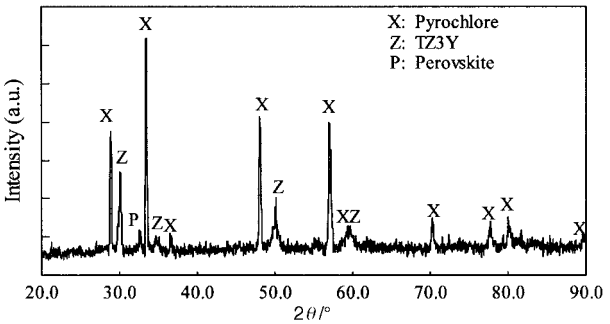

Fig. 3 A representative XRD pattern from the substrate originally in contact with PSM-C showing that the pyrochlore phase was formed after 24 h at 1400 °C.

when the layer was formed with PSM-A, 3.1 μm with PSM-B and 12.0 μm with PSM-C after heat treatment at 1400 °C for 24 h.

In addition to the pyrochlore phase, a second reaction layer was also observed from the fractured surface. Fig. 4 shows a

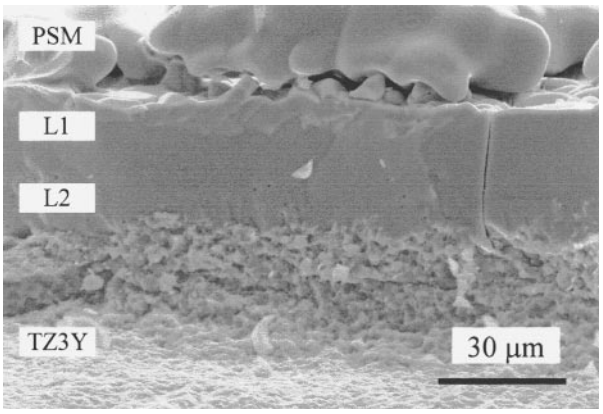

Fig. 4 SEM micrograph of the fractured surface of PSM-A/TZ3Y showing a *ca.* 28 μm thick distinct reaction layer formed between PSM-A and TZ3Y after 24 h at 1400 °C, which consists actually of two layers of products, 'L1' (pyrochlore) and 'L2' (Pr- and Mn-diffused zirconia).

representative micrograph of the fractured surface of PSM-A/TZ3Y. In this micrograph a 28 μm thick distinct layer is obvious between PSM-A and TZ3Y. It contains the pyrochlore layer 'L1' that is only 9.5 μm thick, and another reaction layer 'L2'. The technique of energy dispersive X-ray mapping was used to identify elements in the layer 'L2'. Fig. 5 displays X-ray maps recorded from the polished cross section of PSM-A/TZ3Y showing the distribution of related elements Zr, Y, Sr, Pr and Mn around the interface. It should be noted that the Mn K_α peak partly overlapped with Pr $L_{\beta 2}$, the intensity of which has been subtracted from Mn K_α in Fig. 5. In order to show clearly the element distribution in layer 'L2', X-ray maps (g) and (h) do not include the PSM layer because the contrast between the Mn concentration in PSM and in 'L2' is so high that the Mn distribution in 'L2' can not be seen from Fig. 5(f) when the PSM layer is included. From Fig. 5, it can be seen that the layer 'L2' consists of Pr, Mn and the elements of TZ3Y. The Pr ions and some Mn ions appeared to have entered the TZ3Y lattice forming a solid solution. More results about the nature of this diffusion layer will be presented in the following sections.

The XRD, SEM and EDS observations thus far for

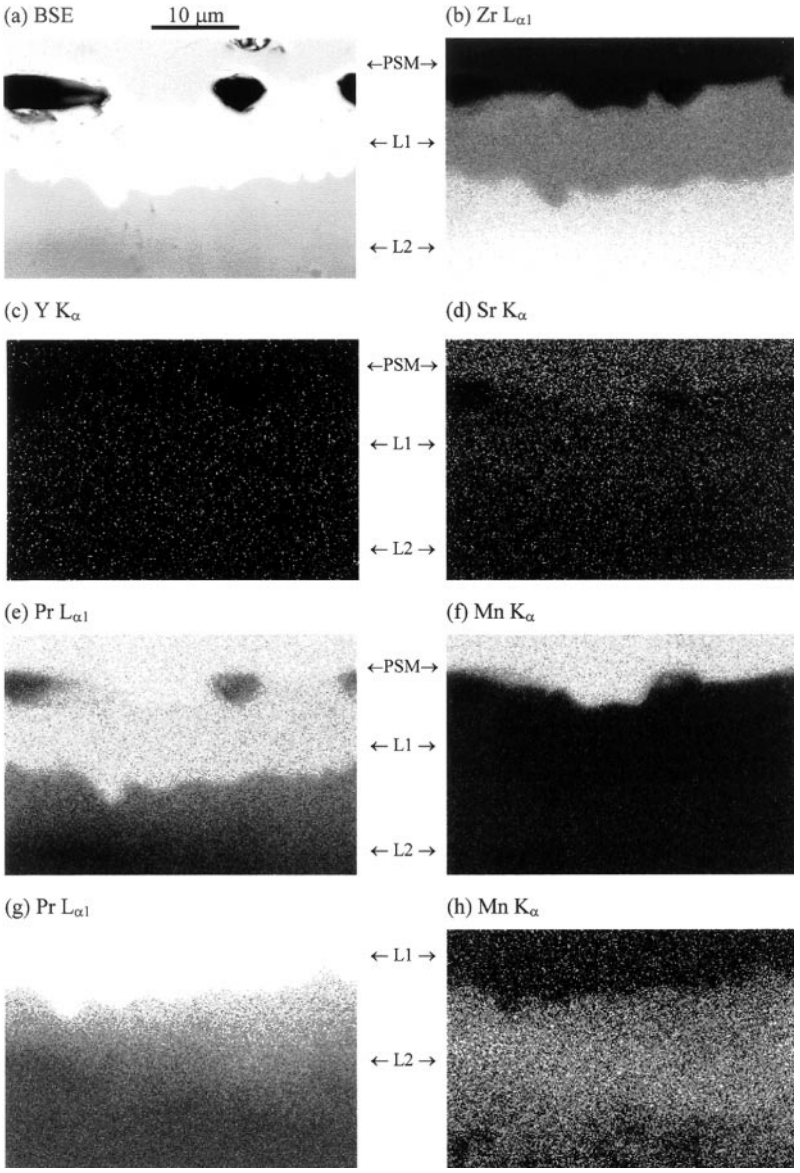

Fig. 5 The EDS X-ray maps recorded from the polished cross section of PSM-A/TZ3Y after 24 h at 1400 °C showing the distribution of related elements in PSM and reaction layers L1 and L2: (a) backscattered electron image; (b) Zr $L_{\alpha 1}$; (c) Y K_α; (d) Sr K_α; (e) Pr $L_{\alpha 1}$; (f) Mn K_α. The X-ray maps (g) Pr $L_{\alpha 1}$ and (h) Mn K_α do not include the PSM layer in order to show clearly the distribution of Pr and Mn in the diffusion layer 'L2', which can not be seen clearly from (e) and (f) in which the PSM layer is included.

Table 1 The thickness of the zirconate layer and the diffusion distance of Pr and Mn in TZ3Y after 24 h at 1400 °C

Specimen	Thickness of zirconate/μm	Pr diffusion distance[a]/μm	Mn diffusion distance[a]/μm
PSM-A/TZ3Y	9.5	28	55
PSM-B/TZ3Y	3.1	6	14
PSM-C/TZ3Y	12.0	30	70

[a]The distance was measured from the PSM/pyrochlore phase interface.

PSM-A/TZ3Y interface heat treated at 1400 °C can be summarised as below.

1 Pr ions have diffused into TZ3Y. The diffusion distance is about 28 μm (from the PSM/pyrochlore interface), corresponding to the thickness of the dense layer viewed from the fractured surface.

2 Mn ions have also diffused into TZ3Y. The diffusion distance of Mn ions (*ca.* 55 μm from PSM) is much larger than that of Pr. However, Mn was not detected in the praseodymium zirconate layer.

3 A small amount of Sr, estimated to be less than a few wt.%, was also detected in the zirconate layer (L1), but no strontium zirconate phase was formed.

4 Zr or Y was not found in the PSM phase. XRD study showed that the perovskite phase of the PSM layer did not change its structure after the reaction.

5 The yttrium was detected in both reaction layers (L1 and L2) at about the same level as in the TZ3Y bulk phase (*i.e.* 3 mol% Y_2O_3).

The same microstructure of the interface was also found in the other two specimens PSM-B/TZ3Y and PSM-C/TZ3Y heat-treated at 1400 °C for 24 h. The thickness of the zirconate and the diffusion distance (measured from the PSM/pyrochlore interface) of the major elements Pr and Mn in TZ3Y in three specimens are summarised in Table 1. It can be seen from Table 1 that the degree of the reaction for PSM-A/TZ3Y is slightly lower than that for PSM-C/TZ3Y interface whereas PSM-B/TZ3Y interface showed relatively higher stability.

The fact that Zr and Y were not detected in the PSM layer, clearly indicates that the growth of the zirconate layer is in the direction of the abutting electrolyte. This was also obvious from Fig. 6, a micrograph taken from the cross section of PSM-A/TZ3Y after 24 h at 1400 °C. In the area where there was no PSM-A, the pyrochlore phase was not formed. It can be seen from the micrograph that the TZ3Y substrate and the praseodymium zirconate top surfaces are almost level, indicating that the zirconate phase has grown into the TZ3Y substrate. The absence of PSM-A in such areas probably arose from the shrinkage of the coating at high temperature.

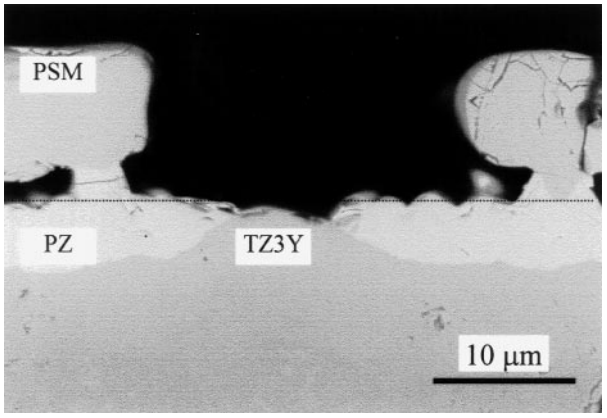

Fig. 6 SEM micrograph from the cross section of PSM-A/TZ3Y after 24 h at 1400 °C showing that the TZ3Y substrate and the praseodymium zirconate top surfaces are almost leveled, indicating that the zirconate has grown into the TZ3Y substrate.

It was also noticed from SEM examination that the PSM-A and PSM-C coatings were highly sintered compared with the PSM-B coating.

(2) Reaction products after heat treatment at 1200 °C

Fig. 7 displays the backscattered electron micrographs of polished cross sections of PSM-A/TZ3Y, PSM-B/TZ3Y and PSM-C/TZ3Y after heat treatment at 1200 °C for 4, 24 and 168 h respectively. The top part in each micrograph shows PSM, and the bottom section the substrate. Pyrochlore (PZ) formed at the interface is marked on the micrographs. From these micrographs it can be seen that the reaction products between PSM and TZ3Y vary with the A-site stoichiometry of PSM and the time of heat treatment. Substantial amounts of praseodymium zirconate were detected after heat treatment of PSM-A/TZ3Y at 1200 °C for 168 h, PSM-B/TZ3Y for 24 h, and PSM-C/TZ3Y for 4 h. In PSM-B/TZ3Y and PSM-C/TZ3Y, praseodymium zirconate formed a continuous layer at the interface, whereas in PSM-A/TZ3Y the zirconate formed islands at contact points between PSM-A and the substrate. The thickness of the reaction layer grew with the time of heat treatment.

The inset in the micrograph of PSM-C/TZ3Y/24 h in Fig. 7 is an enlargement of the reaction layer, showing clearly two distinct layers of products between the PSM-C coating and the substrate. Fig. 8 presents the EDS spectra (a) for the top layer (the brightest in contrast in the micrograph) and (b) for the bottom layer, showing that both layers contain Pr and Zr but with different atomic ratios. The experimental conditions for the EDS X-ray analysis were kept the same in all cases so that a semi-quantitative comparison of elemental concentration in different specimens could be carried out. Trace (b) in Fig. 8 is a typical EDS spectrum of praseodymium zirconate. From comparison of the two EDS traces it is known that the atomic ratio of Pr/Zr of the top layer is higher than that of the pyrochlore layer which is about 1 : 1. The top layer, therefore, consists of a $(Pr,Zr)O_x$ phase with the atomic ratio of $Pr/Zr > 1$. A very thin layer of $(Pr,Zr)O_x$ phase was also detected in PSM-C/TZ3Y after 4 h at 1200 °C when it was examined at a higher magnification. After 168 h at 1200 °C the amount of $(Pr,Zr)O_x$ was much less than that after 24 h, and did not form a distinct layer, as shown in Fig. 7.

After removal of most of the PSM-C coating from the specimen sintered for 24 h at 1200 °C, XRD analysis was carried out on the substrate and part of the trace is displayed in Fig. 9. There are a few extra peaks (marked 'O') in the XRD trace besides those of expected phases pyrochlore, TZ3Y and perovskite (left over from scraping). These extra reflections are probably of the $(Pr, Zr)O_x$ solid solution phase because they match with the reflections of Pr_6O_{11} with a systematic peak position shift (to larger angle) that is not a zero point error.

The Pr and Mn diffusion layer observed in the specimens sintered at 1400 °C was also detected in all specimens heated at 1200 °C. Some representative EDS spectra of the diffusion layer are displayed in Fig. 10. Spectra (a) and (b) were recorded from the diffusion layers formed in PSM-A/TZ3Y after heat treatment for 4 and 24 h respectively at 1200 °C, showing clearly the presence of Pr and Mn in TZ3Y. For comparison the EDS spectrum of praseodymium zirconate formed in PSM-A/TZ3Y after 168 h is also displayed in Fig. 10(c). It can be seen from Fig. 10 that the concentration of Pr in TZ3Y increases with the time of heat treatment.

The diffusion layer is not obvious from the contrast of SEM micrographs taken from polished cross sections (Fig. 7). However, the change of the substrate microstructure near the interface due to diffusion of Pr and Mn and the formation of the pyrochlore phase can be seen on the substrate surface by removing the PSM coating carefully from the substrate. This is illustrated in the secondary electron micrographs shown in Fig. 11. Fig. 11(a) was taken from the unreacted TZ3Y for

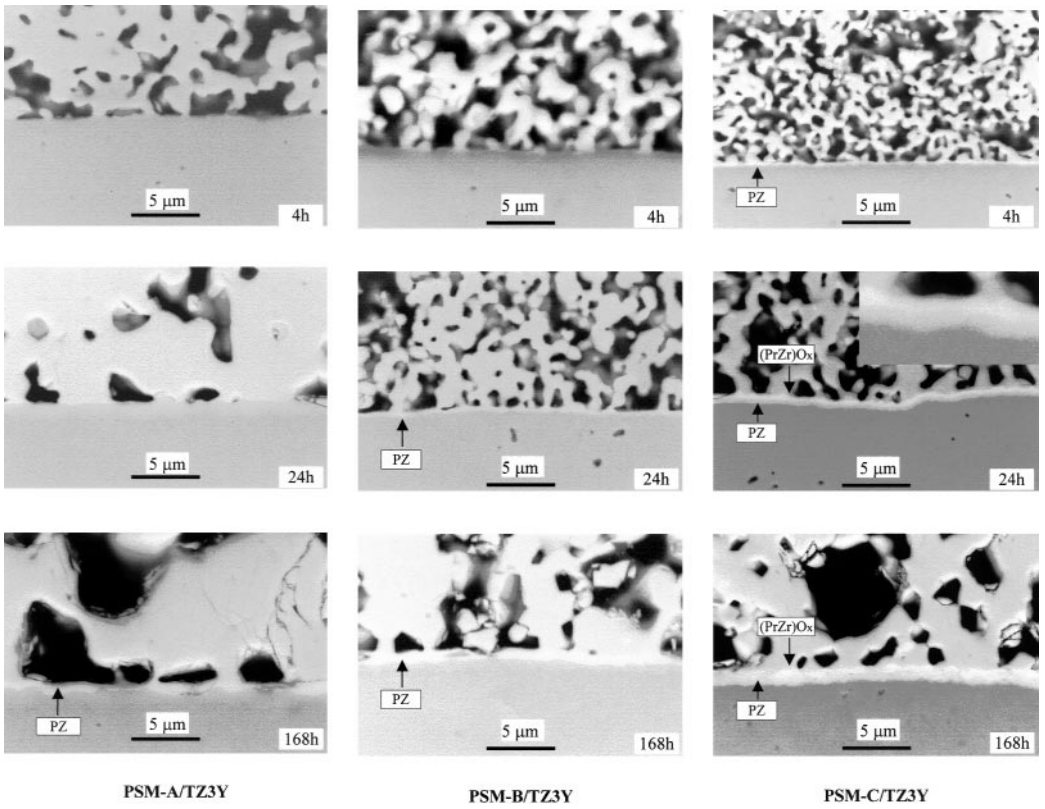

Fig. 7 The backscattered electron micrographs of the polished cross sections of PSM-A/TZ3Y, PSM-B/TZ3Y and PSM-C/TZ3Y after heat treatment at 1200 °C for 4, 24 and 168 h respectively. The top part in each micrograph shows PSM, and bottom part the substrate. Pyrochlore (PZ) formed at the interface is marked in the micrographs. The inset in the micrograph of PSM-C/TZ3Y/24h is an enlargement of the reaction layer, showing clearly two distinct layers of products between the PSM-C coating and the substrate.

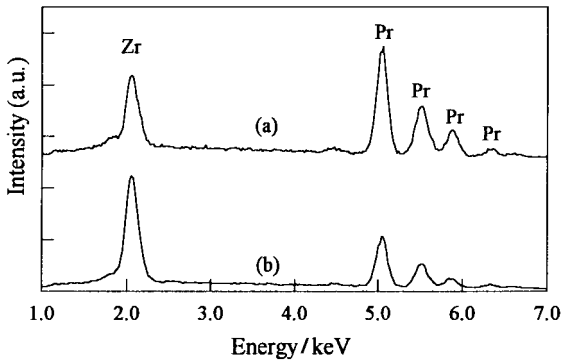

Fig. 8 The EDS spectra recorded from the top layer (a) and the bottom layer (b) shown as inset in the micrograph PSM-C/TZ3Y/24 h in Fig. 7, indicating that both layers contain Pr and Zr but with different atomic ratios.

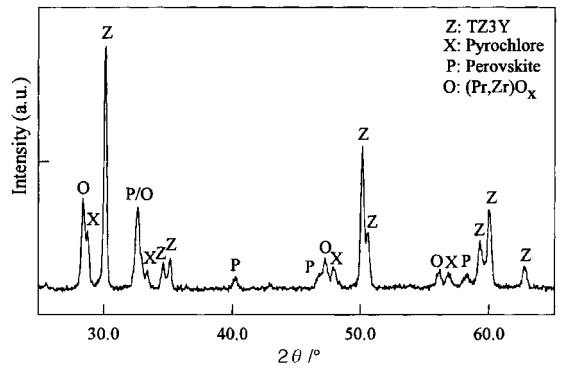

Fig. 9 The XRD pattern recorded from the substrate surface of PSM-C/TZ3Y after 24 h at 1200 °C showing the formation of the praseodymia solid solution $(Pr,Zr)O_x$ besides the expected phases pyrochlore, TZ3Y and perovskite.

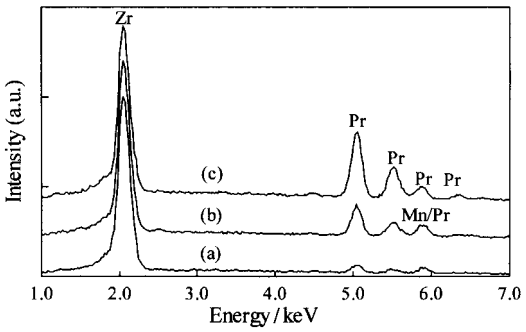

Fig. 10 The EDS spectra recorded from the substrate near the interface of PSM-A/TZ3Y after sintering at 1200 °C for 4 h (a), 24 h (b) and 168 h (c). The electron beam was located on the zirconate for spectrum (c).

comparison; Fig. 11(b) from the Pr- and Mn-diffused zirconia in PSM-A/TZ3Y showing a dramatic increase of the grain size of zirconia near the interface after 24 h at 1200 °C; Fig. 11(c) from the same specimen as in Fig. 11(b) but in a different area showing the trace of some contact points with PSM; Fig. 11(d) from the praseodymium zirconate surface formed in PSM-A/TZ3Y after heat treatment at 1200 °C for 168 h; and Fig. 11(e) from the substrate surface near the edge of the reaction layer in PSM-B/TZ3Y after heat treatment at 1200 °C for 168 h showing the microstructure of different layers including the pyrochlore layer 'L1', the Pr- and Mn-diffused zirconia layer 'L2' and the unreacted TZ3Y. EDS analysis on the trace of the contact points shown in Fig. 11(c) showed a typical composition of the pyrochlore phase. This indicates that some crystal nuclei of praseodymium zirconate had been formed on the surface of Pr- and Mn-diffused zirconia in PSM-A/TZ3Y after 24 h at 1200 °C. The crystal nuclei of praseodymium zirconate were not observed from the cross-section in Fig. 7 probably because the scale is too small.

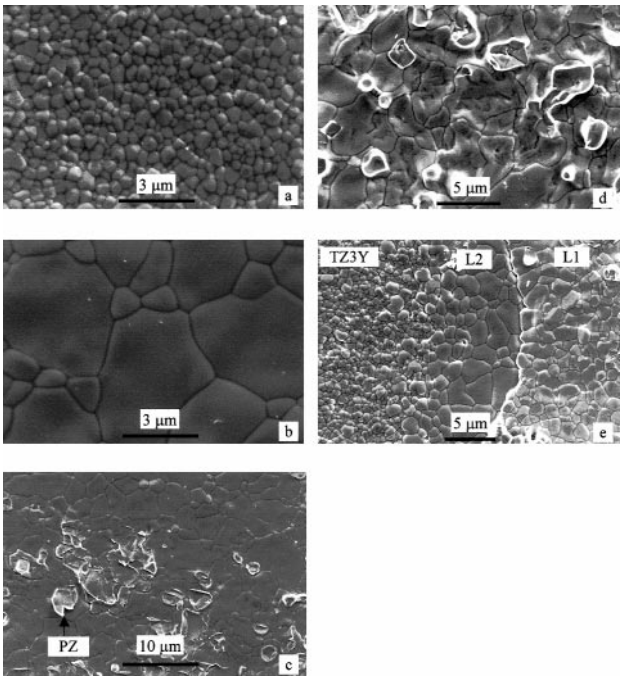

Fig. 11 SEM micrographs showing the morphology of the substrate surface: (a) unreacted TZ3Y; (b) the Pr- and Mn-diffused zirconia in PSM-A/TZ3Y showing a dramatic grain growth of zirconia at the interface after 24 h at 1200 °C; (c) the same specimen as (b) but in a different area showing the formation of the pyrochlore crystal nuclei; (d) the praseodymium zirconate surface formed in PSM-A/TZ3Y after sintering at 1200 °C for 168 h; and (e) the substrate surface near the edge of the reaction layer in PSM-B/TZ3Y after 168 h at 1200 °C showing the microstructure of different layers including the pyrochlore layer 'L1', the Pr- and Mn-diffused zirconia layer 'L2' and the unreacted TZ3Y.

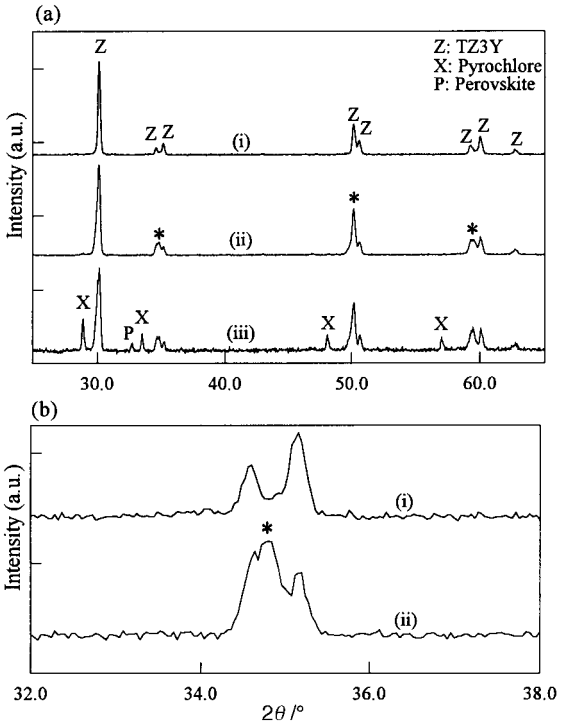

Fig. 12 (a) The XRD patterns recorded from the substrate surface: (i) unreacted TZ3Y, (ii) reacted with PSM-A at 1200 °C for 24 h and (iii) reacted for 168 h. (b) Enlarged part of (a) showing that the reflection marked * in (ii) consists of two peaks.

Fig. 12(a) displays the XRD patterns recorded from the substrate surface: (i) unreacted TZ3Y, (ii) reacted with PSM-A at 1200 °C for 24 h and (iii) reacted for 168 h. The TZ3Y has a tetragonal form of crystal structure, and the trace (i) in Fig. 12(a) is a typical XRD pattern of a tetragonal zirconia. A comparison between the trace (ii) and the trace (i) shows that the relative intensities of a number of reflections (marked with an asterisk) in trace (ii) are much higher than in trace (i). In fact, when the traces were enlarged, it was observed that each of the enhanced reflections consisted of two peaks, and one example is shown in Fig. 12(b). This suggests that another phase has been formed with the diffusion of Pr and/or Mn ions into the zirconia. Trace (iii) in Fig. 12(a) is composed of the diffraction peaks belonging to the Pr- and Mn-diffused zirconia shown in the trace (ii) and those of pyrochlore phase. All XRD results are consistent with SEM observations.

In order to characterise the phase of the Pr- and Mn diffused zirconia, the XRD data of trace (ii) in Fig. 12(a) were analysed using the Rietveld method. During the Rietveld refinement the unit cell parameters, zero point, scale factors, peak width/shape/asymmetry parameters and background coefficients were refined simultaneously to convergence. The atomic position parameters were fixed as reported in the literature.[19] When the structure parameters of tetragonal zirconia were tested in the Rietveld refinement, the agreement index R_{wp} was 0.132. When the cubic as well as the tetragonal lattice of zirconia was used in the refinement, R_{wp} dropped significantly to 0.068. The output from the Rietveld refinements using (a) the tetragonal lattice, and (b) the cubic as well as the tetragonal lattice is displayed in Fig. 13. Large difference (lower curve in each figure) in reflection intensities between the observed (+ markers) and the calculated (continuous line) XRD profiles was observed from Fig. 13(a) when only a tetragonal lattice was used for the refinement. The fit, however,

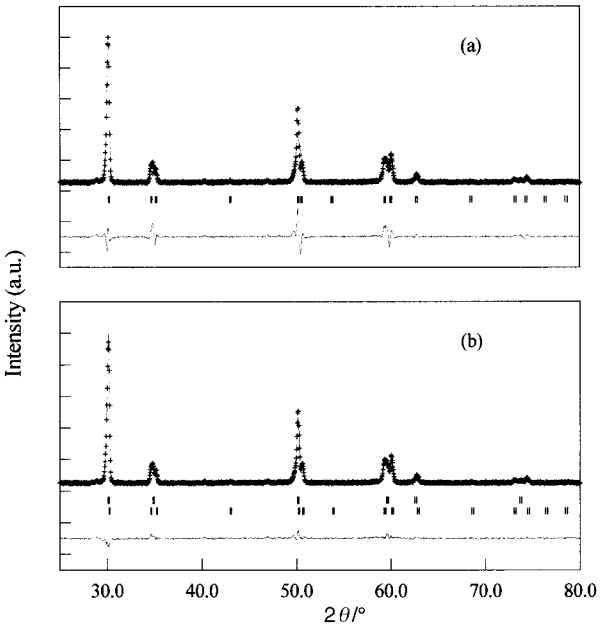

Fig. 13 The output from the Rietveld refinements of the XRD pattern of the Pr- and Mn-diffused TZ3Y in PSM-A/TZ3Y after 24 h at 1200 °C using (a) tetragonal lattice, and (b) cubic as well as tetragonal lattice. The observed data are indicated by crosses and the calculated by a continuous line overlying them, and the difference profile is the lower curve in each figure. The short vertical lines show the positions of all possible Bragg reflections.

was improved significantly when the cubic lattice was included in the refinement, as shown in Fig. 13(b). This suggests that the Pr- and Mn-diffused zirconia region has a cubic structure and is consistent with the observation of grain growth in the diffusion layer because usually dopant-stabilised cubic zirconia has much larger grain size than tetragonal TZ3Y.

The alteration of the crystal structure from tetragonal to

Table 2 A summary of reaction products between PSM and TZ3Y at 1200 °C

	Products		
Specimen	4 h	24 h	168 h
PSM-A/TZ3Y	Diffusion layer[a]	$Pr_2Zr_2O_7$ nuclei Diffusion layer	$Pr_2Zr_2O_7$ islands Diffusion layer
PSM-B/TZ3Y	Diffusion layer	$Pr_2Zr_2O_7$ layer Diffusion layer	$Pr_2Zr_2O_7$ layer Diffusion layer
PSM-C/TZ3Y	$(Pr,Zr)O_x$ layer $Pr_2Zr_2O_7$ layer Diffusion layer	$(Pr,Zr)O_x$ layer $Pr_2Zr_2O_7$ layer Diffusion layer	$(Pr,Zr)O_x$ islands $Pr_2Zr_2O_7$ layer Diffusion layer

[a]Diffusion layer refers to Pr- and Mn-diffused zirconia layer.

cubic indicates that at least part of the Pr and Mn ions have entered the lattice of zirconia.

The interfacial reaction products between TZ3Y and PSM of three compositions at 1200 °C are summarised in Table 2.

4 Discussion

The above results can be summarised as follows.

1 A diffusion layer of Pr and Mn in zirconia was formed in all specimens regardless of the A-site stoichiometry and the heat treatment temperature. The Pr- and Mn-diffused zirconia is cubic and its grain size is much larger than that in TZ3Y.

2 The pyrochlore phase was formed at the interface of PSM with Pr- and Mn-diffused zirconia after heat treatment at 1200 °C for different times for all compositions of PSM studied. Significant amounts of pyrochlore phase were detected after 168 h in PSM-A/TZ3Y, after 24 h in PSM-B/TZ3Y and after 4 h in PSM-C/TZ3Y.

3 Besides the pyrochlore phase, a Pr-rich $(Pr,Zr)O_x$ phase was detected at the interface of the A-site over-stoichiometric PSM-C/TZ3Y. The $(Pr,Zr)O_x$ phase formed a distinct layer after 24 h of heat treatment at 1200 °C, and was much less conspicuous after 168 h.

4 Relatively thick layers of pyrochlore phase were formed after 24 h at 1400 °C for all compositions of PSM in contact with TZ3Y. The degree of the reaction for PSM-B/TZ3Y was much lower than that for PSM-A/TZ3Y and PSM-B/TZ3Y.

The dissolution of Pr ions in TZ3Y can be understood from the phase relations between zirconia and praseodymia. Zirconia can react with praseodymia, forming solid solutions varying from tetragonal zirconia, cubic zirconia, pyrochlore phase to praseodymia with the increase of the praseodymia content at 1600 °C.[20] The solid state reactions between zirconia and praseodymia at 900 and 1100 °C have also been reported.[21] The current study has shown that Pr ions can enter the lattice of zirconia at 1200 and 1400 °C and form a cubic phase of zirconia solid solution. The Pr concentration increased in the cubic zirconia with the heating time. When the solubility limit of Pr ions in cubic zirconia was reached, the pyrochlore phase crystallised out.

In the A-site over-stoichiometric PSM-C coating, a considerable amount of free praseodymium oxide is present, which reacted with TZ3Y when heat treated at high temperature. A gradation of Pr concentration from the Pr_6O_{11}/TZ3Y interface (high) to the Pr-diffused zirconia (low) is expected. Therefore, various layers ranging from $(Pr,Zr)O_x$ with atomic ratio of $Pr/Zr > 1$, the pyrochlore with $Pr/Zr \cong 1$, to the diffusion layer with $Pr/Zr < 1$, were formed between PSM and TZ3Y at 1200 °C. However, when the free Pr_6O_{11} was consumed, no further $(Pr,Zr)O_x$ phase was formed. The Pr ions from the $(Pr,Zr)O_x$ solid solution, which contains the highest Pr concentration in the specimen, would diffuse through the pyrochlore layer and react with more zirconia. Therefore, the amount of $(Pr,Zr)O_x$ solid solution after 168 h was less than that after 24 h at 1200 °C. It is expected to eventually disappear completely.

In PSM-A and PSM-B, there was no free praseodymia in the coating. The atomic ratio of $Pr/Zr > 1$ at the interface with TZ3Y was unlikely to occur, and therefore, the Pr-rich phase $(Pr,Zr)O_x$ was not formed.

The formation of pyrochlore phase was delayed in PSM-A/TZ3Y and PSM-B/TZ3Y. It has been reported before that A-site deficiency in the perovskite may suppress or delay the formation of pyrochlore phase in the LSM/YSZ system.[4,6,11,13] This was explained by the hypothesis that the diffusion of Mn into YSZ produced chemically active La_2O_3, which formed pyrochlore phase with YSZ. Therefore, extra manganese in the perovskite should suppress the formation of free La_2O_3, and hence the pyrochlore phase. However, this hypothesis cannot explain why the formation of pyrochlore phase was delayed in PSM-B/TZ3Y with no excess Mn in the perovskite. Furthermore, the results of the current study showed clearly that the Pr and Mn ions had diffused into zirconia, regardless of the stoichiometry of PSM. The chemically active praseodymia was unlikely to have been produced during the interaction. It seems that a different explanation is required to understand the delay for the formation of the pyrochlore phase in PSM-A/TZ3Y and PSM-B/TZ3Y.

From the phase relations, it is known that the pyrochlore phase is formed only when the local Pr concentration has reached the solubility limit in cubic zirconia. When there was no extra praseodymia in the PSM coating as in PSM-A/TZ3Y and PSM-B/TZ3Y, the atomic ratio of Pr/Zr was initially very low in zirconia in the area near the interface. With time more Pr ions diffused into the region near the interface. Some of it diffused out into an area in zirconia further away from the interface due to the gradation of Pr concentration. It would therefore take some time at 1200 °C for the Pr ions to reach the solubility limit in cubic zirconia in the area near the interface. Accordingly, the formation of the pyrochlore phase was delayed in PSM-A/TZ3Y and PSM-B/TZ3Y. As the Pr content in PSM-A was lower than in PSM-B, the migration of Pr ions from PSM-A to TZ3Y is therefore expected to be slower than from the stoichiometric PSM-B during the initial stage of heat treatment. Therefore the delay for forming pyrochlore phase with PSM-A was more pronounced than that with PSM-B at 1200 °C.

At 1400 °C the whole process was accelerated. A complete layer of pyrochlore phase was formed for all specimens after 24 h. It needs to be noted that different from the observations at 1200 °C, the amount of pyrochlore phase formed with PSM-A at 1400 °C is much more than with PSM-B. This may be explained from the change of the migration rate of Pr ions at various stages of heat treatment and in particular, the difference in PSM/substrate contact areas between the two specimens. As the Mn content in PSM-A was higher than in PSM-B, the migration of Mn ions from PSM-A to zirconia is expected to be faster than from PSM-B during the initial stage of heat treatment. On the other hand, the higher Pr content in PSM-B resulted in a further migration of Pr ions from PSM-B to zirconia. This means that more Mn ions would leave from PSM-A than from PSM-B and more Pr ions would leave from

PSM-B than from PSM-A. It is quite likely that after some time of heat treatment (the initial stage), the chemical compositions for PSM-A and PSM-B may become somewhat similar. After this initial stage, the amount of the pyrochlore formed between PSM and the substrate will be primarily determined by the contact area between the two materials. A large contact area, as present in PSM-A (Fig. 2), will lead to enhanced Pr migration from PSM to the substrate. This mechanism would explain the fact that the pyrochlore layer formed with PSM-A after 24 h at 1400 °C is thicker than with PSM-B.

It appears that at the initial stage of heat treatment, the amount of Pr ions migrating into TZ3Y was determined mainly by the A-site stoichiometry of the perovskite. The composition difference between the different perovskites may disappear after the initial stage of the heat treatment is complete. The amount of Pr ions diffusing into the substrate was then determined mainly by the contact area between PSM and the substrate. It seems that the initial stage is complete after 24 h at 1400 °C but not yet after 168 h at 1200 °C for all the compositions of PSM.

The relatively large contact area between PSM-A and the substrate may be attributed to the high sinterability for the A-site deficient perovskite. This has been observed previously by other authors.[13] It was assumed that the vacancy within the structure of the A-site deficient perovskite enhanced the cation diffusion in perovskite itself and hence improved the sinterability of the perovskite.

The highest reaction degree for PSM-C at 1400 °C among all the diffusion couples can be attributed to the presence of free Pr_6O_{11} at the initial stage as well as to the high contact area between PSM-C and the substrate.

Mn was always detected in the diffusion layer in the current study. It appears that both Pr and Mn migrate out of the PSM electrode (for all compositions) into the electrolyte. However, some Pr is trapped by the formation of the pyrochlore phase, while Mn keeps on diffusing into zirconia. This may explain much deeper diffusion zone for Mn than that for Pr even after longer heat treatment times. There is no consistency in the literature about the manganese diffusion in yttria stabilised zirconia. Some authors have reported manganese diffusion in zirconia,[3,6,22,23] whereas others did not detect any Mn in zirconia.[4,8,12] Waller *et al.* recently studied the manganese diffusion in single crystal and polycrystalline yttria stabilised zirconia using XRD and dynamic secondary ion mass spectrometry techniques, and showed convincingly that Mn ions have diffused into both single crystal and polycrystalline zirconia.[24] The diffusion coefficient of Mn in polycrystalline zirconia was significantly higher than that in the single crystal. They concluded that in polycrystalline zirconia, the grain boundary diffusion of Mn dominates the mechanism for Mn migration into zirconia. The substrate used in the current study is polycrystalline TZ3Y that has a much higher density of grain boundaries to provide diffusion paths for manganese than the 7.5 mol% yttria stabilised zirconia used by Waller *et al.*[24] Therefore, a considerable amount of manganese diffusion into TZ3Y at both 1200 and 1400 °C is expected as indeed was the case in the present study.

5 Conclusions

The interfacial reactions between $(Pr_{0.8}Sr_{0.2})_yMnO_3$ electrode, with different A-site stoichiometry, and TZ3Y electrolyte at 1200 and 1400 °C in air have been studied. It has been found that both Pr and Mn ions diffused into TZ3Y forming a cubic zirconia solid solution. When the solubility limit of Pr ions in the cubic zirconia was reached, a pyrochlore phase was formed. When there was free praseodymia in the PSM coating, a praseodymia–zirconia solid solution $(Pr,Zr)O_x$ was formed, which occurred only in the case of the $(Pr_{0.8}Sr_{0.2})_{1.05}MnO_3$/TZ3Y couple. The solubility limit of Pr in zirconia for specimens $(Pr_{0.8}Sr_{0.2})MnO_3$/TZ3Y and $(Pr_{0.8}Sr_{0.2})_{0.9}MnO_3$/TZ3Y were reached after much longer time compared with $(Pr_{0.8}Sr_{0.2})_{1.05}MnO_3$/TZ3Y. The formation of the pyrochlore phase, therefore, was delayed in these two specimens at 1200 °C. The amount of the pyrochlore phase formed at the interface was determined by the A-site stoichiometry of PSM in the initial stages of heat treatment. The growth of the pyrochlore layer after the initial stage, however, appeared to be controlled by the contact area between PSM and the substrate. It is believed that the initial stage is complete after 24 h at 1400 °C but not even after 168 h at 1200 °C for all the compositions of PSM. The A-site deficient $(Pr_{0.8}Sr_{0.2})_{0.9}MnO_3$ in contact with TZ3Y, following long term heat treatment, will form more pyrochlore phase than the stoichiometric $(Pr_{0.8}Sr_{0.2})MnO_3$ due to the large contact area between PSM-A and TZ3Y.

Acknowledgements

The authors are grateful to Dr. R. Ratnaraj and Mr. K. Wilshier for reviewing this paper, Mr. D. Milosevic for synthesising the PSM powders, Mr. R. Donelson for supplying the TZ3Y substrates, Mr. H. Jaeger for assistance with microscopy, Natasha Rockelmann with XRD, and Kristine Giampietro and Kylie Chapman with specimen and micrograph preparation.

References

1 N. Q. Minh, *J. Am. Ceram. Soc.*, 1993, **76**, 563.
2 S. P. S. Badwal and K. Foger, *Mater. Forum*, 1997, **21**, 183.
3 L. Kindermann, D. Das, D. Dahadur, R. Weiß, H. Nickel and K. Hilpert, *J. Am. Ceram. Soc.*, 1997, **80**, 909.
4 A. Mitterdorfer, M. Cantoni and L. J. Gauckler, in *Second European Solid Oxide Fuel Cells Forum*, ed. B. Thorstensen, Druckerei J. Kinzel, Gottingen, 1996, p. 373.
5 D. Kuscer, J. Holc, M. Hrovat, S. Bernik, Z. Samardzija and D. Kolar, *Solid State Ionics*, 1995, **78**, 79.
6 G. Stchniol, E. Syskakis and A. Naoumidis, *J. Am. Ceram. Soc.*, 1995, **78**, 929.
7 H. Taimatsu, K. Wada and H. Kaneko, *J. Am. Ceram. Soc*, 1992, **75**, 401.
8 C. Brugnoni, U. Ducati and M. Scagliotti, *Solid State Ionics*, 1995, **76**, 177.
9 G. Stochniol, H. Grubmeier, A. Naoumidis and H. Nickel, in *Proceedings of the Fourth International Symposium on Solid Oxide Fuel Cells (SOFC-IV)*, ed. M. Dokiya, O. Yamamoto, H. Tagawa and S. C. Singhal, The Electrochemical Society, Pennington, NJ, 1995, p. 995.
10 C. Clausen, C. Bagger, J. B. Bilde-Sorensen and A. Horsewell, *Solid State Ionics*, 1994, **70/71**, 59.
11 T. Tsepin and S. A. Barnett, *Solid State Ionics*, 1997, **93**, 207.
12 J. A. M. van Roosmalen and E. H. P. Cordfunke, *Solid State Ionics*, 1992, **52**, 303.
13 J. W. Stevenson, T. R. Armstrong and W. J. Weber, in ref. 9, p. 454.
14 H. Y. Lee and S. M. Oh, *Solid State Ionics*, 1996, **90**, 133.
15 T. Ishihara, T. Kudo, H. Matsuda and Y. Takita, *J. Am. Ceram. Soc*, 1994, **77**, 1682.
16 T. L. Wen, H. Tu, Z. Xu and O. Yamamoto, in *Extended Abstracts of 11th International Conference on Solid State Ionics*, Honolulu, Hawaii, Nov. 16–21, 1997, p. 188.
17 H. M. Rietveld, *J. Appl. Crystallogr.*, 1969, **2**, 65.
18 R. J. Hill and C. J. Howard, Report No. M112, Australian Atomic Energy Commission (now ANSTO), Lucas Heights Research Laboratories, New South Wales, Australia, 1986.
19 C. J. Howard, R. J. Hill and B. E. Reichert, *Acta Crystallogr., Sect. B*, 1988, **44**, 116.
20 R. L. Withers, J. G. Thompson and P. J. Barlow, *J. Solid State Chem.*, 1991, **94**, 89.
21 M. K. Nasakar and D. Ganguli, *J. Mater. Sci.*, 1996, **31**, 6263.
22 A. Khandkar, S. Elangovan and M. Liu, *Solid State Ionics*, 1992, **52**, 57.
23 S. K. Lau and S. C. Singhal, in *Corrosion 85*, The National Association of Corrosion Engineers (NACE) Meeting, Boston, MA, March 25–29, 1985, p. 345/1.
24 D. Waller, J. D. Sirman and J. A. Kilner, in *Proceedings of the Fifth International Symposium on Solid Oxide Fuel Cells (SOFC-V)*, ed. U. Stimming, S. C. Singhal, H. Tagawa and W. Lehnert, The Electrochemical Society, Pennington, NJ, 1997, p. 1140.

Paper 8/05835K